

STUDY OF THE FLOW INSIDE AN INDUSTRIAL ELECTRICAL BREAKER

M. Al-Amayreh¹, S. Ausmeier¹, A. Petchenko¹, A. Delgado¹, H. Iglseder², C. Weindl³, H. Hofmann³, O. Nilsson⁴, R. Kralik⁴, A. Ignatov⁴

1 Lehrstuhl für Strömungsmechanik, Friedrich-Alexander-Universität Erlangen-Nürnberg,
91058 Erlangen, Germany. malik.amayreh@lstm.uni-erlangen.de

2 STMS - Consulting, 31552 Rodenberg, Germany

3 Lehrstuhl für Elektrische Energieversorgung, Friedrich-Alexander-Universität Erlangen-Nürnberg,
91058 Erlangen, Germany

4 Schaltbau GmbH, 81829 München, Germany

Key words: Electrical breaker, Arc Plasma, External magnetic field.

Abstract

This paper investigates the effect of the magnetic field on the arc plasma in an industrial electrical breaker in which the external magnetic field is generated by two coils placed around the plasma runner. A three-dimensional transient computational model of the flow inside the electrical breaker has been carried out taking into consideration a variation of the flow properties with temperature. In addition, an experimental investigation is performed by using optical sensors which were embedded in different parts of the electrical breaker to measure the light of emission. This could help to estimate the time of flight of the arc plasma and its velocity. The flow was turbulent.

The distribution of the magnetic field has been found to be asymmetric due to the appearance of the current in the first coil. The results show that the current density is a function of the area of the arc plasma in addition to the temperature. As the temperature increases, the current density increases due to the increases of the air electrical conductivity. Also the current density decreases with the elongation of the arc plasma.

1. Introduction

The electrical breaker is a mechanical switching device that could carry or break currents under normal current or short circuit conditions (ABB SACE, 2003). In the case of short circuit, the breaker contacts separate from each other, allowing electrical potential difference to accumulate at either side of the contacts, which establishes for an arc plasma. Due to the magnetic field in the breaker the arc plasma is forced to move in a certain path or runner until the arc plasma is finally divided by the splitting plates, as shown in Fig.1. Usually the arc plasma splits into a series of arcs, where the splitting plates work as a quenching system. The velocity profile and the current flow between splitting-plates are studied in Lindmayer et al 2006.

In the present model the internally induced magnetic fields caused by the current flow inside the arc plasma and the breaker contacts in addition to the external magnetic fields. These fields are defined in a vector potential form as expressed in Karetta 1998 et al and Schlitz et al 1999.

The external magnetic field can be generated by ferromagnetic materials or coils. The former case was studied in detail, e.g. by Lindmayer et al 2001, where a simple model of two parallel ferromagnetic materials adhered to the arc chamber is used. In this paper, the main

attention is paid to the case where the magnetic field is generated by coils, i.e. coils 1 and 2 as shown in Fig.1.

As part of the contribution in this paper, a three dimensional model of the arc plasma inside the runners of the electrical breaker is considered. The study is based on a new design of an actual AC/DC electrical breaker described by the patent of Schaltbau company (Kralik 2007). This model exploits the default current to generate a magnetic field from two coils around the runners of the arc plasma. Moreover, the magnetic field is produced by magnetized materials in the base of the electrical breaker, as illustrated in Fig.1.

When a fault current occurs in the circuit, the bridge between plates A1 and B1 moves downwards. The current flows between these plates by an arc plasma established at contact points 1 and 2. The arc moves along line 1 between plate A1 and the bridge, then between A2 and the bridge until it finally elongates between A2 and B2 to continue its path to the splitter plates. During the arc motion between plates A2 and B2 a current will pass through coils 1 and 2. This would induce a magnetic field normal to the flow direction of the arc. A self magnetic field is also induced by the current flow in plates A2 and B2. The self induced magnetic field, the magnetic field from the coils and the magnetic field of the magnetized material are all designed to affect in one direction causing the arc to move in the runner between A2 and B2.

The air plasma thermodynamic coefficients are sensible to temperature at atmospheric pressure. For instance, the electrical conductivity increases with the increase of temperature. In addition, the ablation of the contacts material affects the arc plasma properties. In the simulation of the present work, the specific heat, density, electrical conductivity and viscosity are described as functions of temperature according to the definition used in Swierczynski 2004 et al and Capitelli 2002 et al.

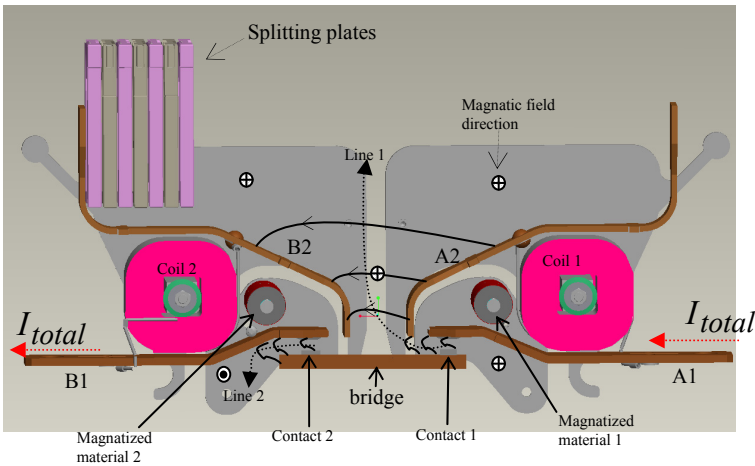


Fig.1 Illustration of the electrical breaker model

2. Mathematical model of the flow inside the electrical breaker

This section provides a review of the MagnetoHydroDynamik (MHD) model. The fluid flow and heat transfer inside the runners of the electrical breaker are described using Maxwell's equations and the principle of conservation of mass, momentum and energy. The Self induced magnetic field is considered beside the magnetic field caused by the coils.

The following assumptions are assumed hold in the present model:

1. No ablation of the contact material.
2. The plasma satisfies the conditions of local thermodynamic equilibrium.
3. Newtonian fluid with unsteady model is considered.
4. The plasma air is assumed as an ideal gas.

The following notations are used to describe the system model: ρ signifies the density, \vec{V} represents the velocity vector, t is the time, \vec{J} is the electric current density, \vec{B} is the magnetic flux density, μ is the dynamic viscosity, h is the enthalpy, k is the thermal conductivity, T is the temperature, Φ is the viscous dissipation, \vec{g} is the gravitational acceleration, p is the pressure, \vec{E} is the electric field, ϕ is the electrical potential, σ is the electrical conductivity and \vec{A} is a three-dimensional vector representing the magnetic potential or $\vec{B} = \nabla \times \vec{A}$.

The continuity and moment equations could be respectively described as (Schlitz et al 1999, Wu et al 2006):

$$\frac{\partial \rho}{\partial t} + \nabla \cdot (\rho \vec{V}) = 0 \quad (1)$$

$$\frac{\partial \rho \vec{V}}{\partial t} + \nabla \cdot (\rho \vec{V} \vec{V}) = \vec{J} \times \vec{B} + \rho \cdot \vec{g} - \nabla p + \nabla \cdot \left[\mu \left(\frac{\partial V_i}{\partial x_j} + \frac{\partial V_j}{\partial x_i} \right) \hat{e}_i \hat{e}_j \right] \quad (2)$$

The arc plasma motion is clearly affected by the Lorentz force given by $\vec{J} \times \vec{B}$ in (2). The last term in (2) is the stress tensor in the Newtonian fluid.

The energy equation could be described by:

$$\frac{\partial \rho h}{\partial t} + \nabla \cdot (\rho \vec{V} h) = \nabla \cdot (k \nabla T) + \frac{\partial p}{\partial t} - Q_r + \vec{J} \cdot \vec{E} + \Phi \quad (3)$$

where $\vec{J} \cdot \vec{E}$ represents the effect of Ohmic heating. The radiation term Q_r is obtained (Karetta et al 1998) in the form $Q_r = 4\alpha \tilde{k} (T^4 - T_o^4)$, with \tilde{k} an absorption coefficient that depends on the wave length, pressure and temperature.

Taking into consideration assumption 4, the equation of state is given in the form:

$$p = \rho RT \quad (4)$$

On the other hand, the current continuity is described as:

$$\nabla \cdot (\sigma \nabla \phi) = 0 \quad (5)$$

Since the electrical field can be written as $\vec{E} = -\nabla \phi$, the current density is related to the electrical potential by:

$$\vec{J} = \sigma \cdot \vec{E} - \sigma \cdot \nabla \phi \quad (6)$$

The simulation in this work is limited to the runners region, i.e. the region between plates A2 and B2, without considering the arc plasma ignition in the base. Therefore, the effect of

the magnetic field from the magnetized material is not considered and the magnetic field can be written as:

$$\vec{B}(\vec{r}) = \vec{B}(\vec{r})_{self-Induced} + \vec{B}(\vec{r})_{left_Coil} + \vec{B}(\vec{r})_{Right_Coil} \quad (7)$$

The self induced magnetic field is calculated from the Biot –Savart equation as:

$$\vec{B}(\vec{r})_{self-Induced} = \frac{\mu_0}{4\pi} \iiint_{V'} J(\vec{r}') \times \frac{\vec{r}'}{|\vec{r}'|^3} dV' \quad (8)$$

Here, \vec{r}' is a vector representing the position of the arc plasma element, and dV' is the differential volume of that element.

The magnetic field from an N -turn coils is perpendicular to the symmetry plane or $z=0$ as described in Fig.2 and Table.1. The value of the external magnetic field B_{coil} apart from the centre of the coils is estimated by Marandi 1996 as:

$$B_{coil} = I_{Coil}(t)K \frac{\mu_0}{4\pi} \frac{b^2 \pi N}{L} R^{-2} \left[\xi_2^3 (R^2 + \xi_2^2)^{-\frac{3}{2}} - \xi_2 (R^2 + \xi_2^2)^{-\frac{1}{2}} \right] - R^{-2} \left[\xi_1^3 (R^2 + \xi_1^2)^{-\frac{3}{2}} - \xi_1 (R^2 + \xi_1^2)^{-\frac{1}{2}} \right] \quad (9)$$

where R is the cylindrical radial distance of the observation point from the axis of the coil, b the radius of the coil, L is the length of the coil, $\mu_0 = 4\pi \times 10^{-7} NA^2$ the permeability of free space, $\xi_2 = \frac{L}{2} - Z$; $\xi_1 = -\frac{L}{2} - Z$ and K is the relative permeability, which depends on the core material of the coil.

3. Grid and Boundary Conditions

The 3-D geometry is adapted from an actual electrical breaker and drawn using ProEngineer. The structured geometry is generated by the programme ICEM. A total of 349520 grid elements were used in the structure form appearing in Fig.2. The mathematical model was solved using the program CFX 11. The boundary equations used in this model are shown in Table 1.

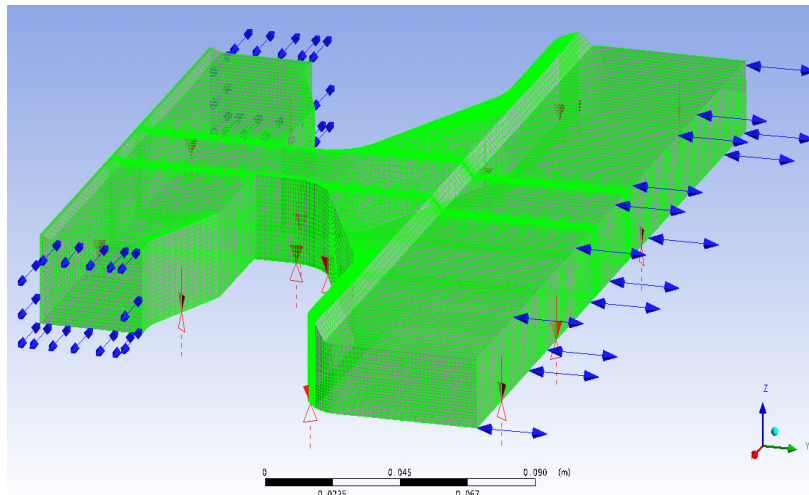
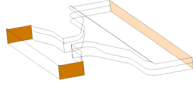

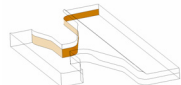
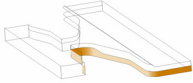
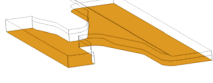


Fig.2 Grid model

Table.1 Boundary conditions

		
<p>Opening Conditions</p> $p = 0, \frac{\partial T}{\partial x_i} = 0, E = 0, A = 0.$	<p>Walls</p> $V_i = 0, \frac{\partial T}{\partial x_i} = 0, J = 0, A = 0$	<p>High Voltage Wall</p> $V_i = 0, \frac{\partial T}{\partial x_i} = 0, A = 0,$ $J = \text{Experimental}.$
		
$V_i = 0, \frac{\partial T}{\partial x_i} = 0, A = 0, \phi = 0.$	Symmetry plane	

4. Experimental Setups

This section describes the main setup used in the experimental part. A schematic diagram of these settings appears in Fig.3 It involves a DC battery that can create up to 480 V, shunt used in current measurement and power resistor for limiting the current. The voltage and the current readings are passed after amplification to a data acquisition unit.

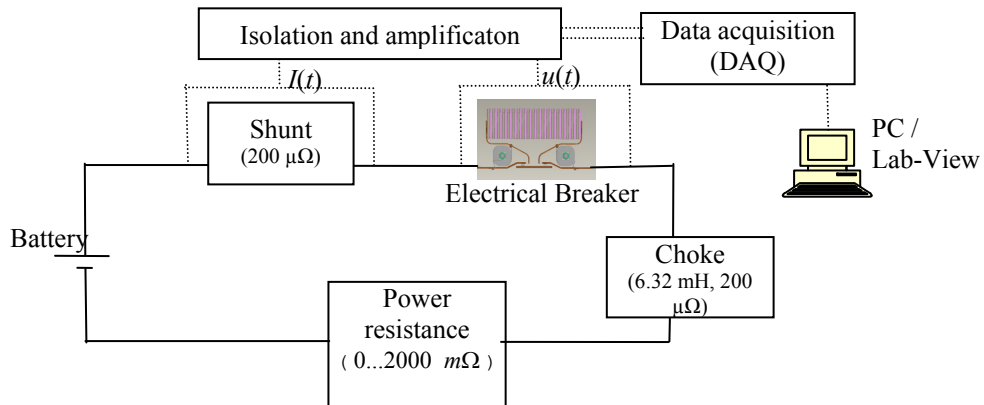


Fig.3 Experimental setup.

In addition to voltage and current measurements, embedded optical sensors, as shown in Fig.4 detect the strength of emitted light inside the electrical breaker, which helps to predict the behaviour of the arc plasma.

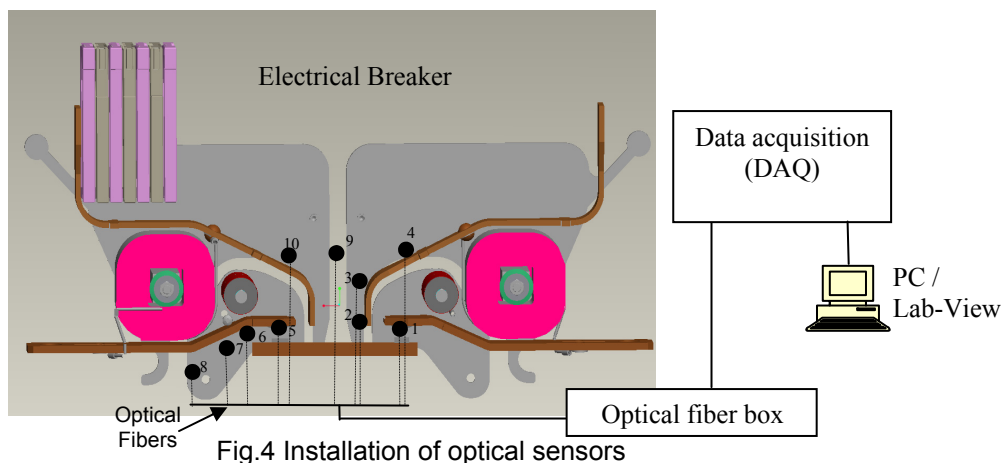


Fig.4 Installation of optical sensors

5. Results

In this part the arc plasma behaviour is presented based on simulations and experimental results obtained for the magnetic field, current and velocity.

5.1 Magnetic field

The magnetic field induced from the coils described in equation (9) is a function of the position and the current inside the coil (I_{Coil}). This current as used in the simulation is based on fitted function derived from real measurements. Such equations and curves are shown for instance in Fig.5 for 25 experimental averages of an default DC current of 755 A, where:

$$I_{Coil1}(t) = 101.7 \exp^{-((t-0.04748[s])/0.003161[s])^2} \tag{10}$$

$$I_{Coil2}(t) = 51.78 \exp^{-((t-0.04893[s])/0.0027[s])^2} \tag{11}$$

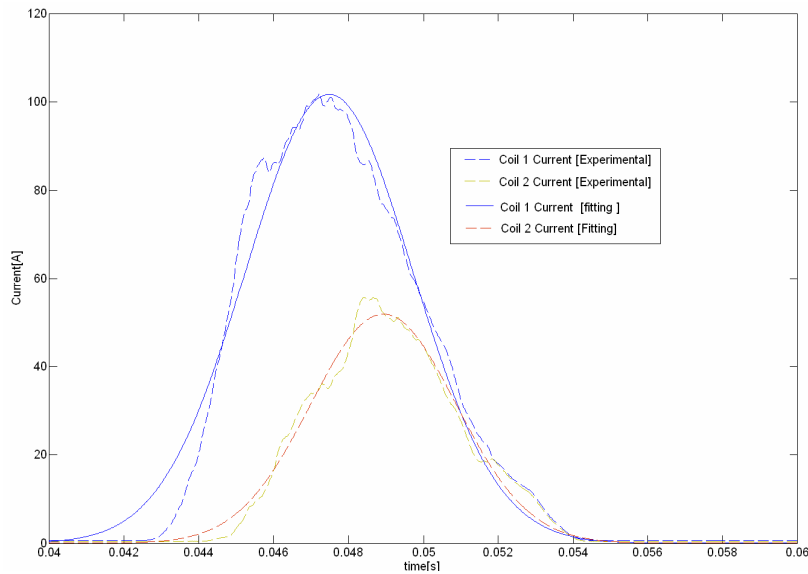


Fig.5 Coils current modelling.

The external magnetic field distribution inside the electrical breaker can be shown in Fig.6 at a time instant. It is obvious that the magnetic field has more concentration near the coils.

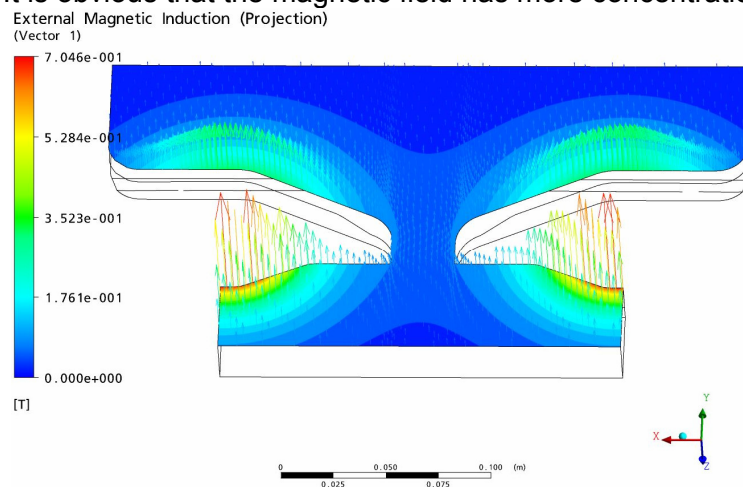


Fig.6 External magnetic field distribution and direction at $t= 48.8$ ms for an initial current of 755 A.

The magnetic field as a function of time is shown at two different points in Fig.7. The total magnetic field is initially dominated by the self-induced field, and then it becomes more affected by the external field as the current flows in the coils. The total magnetic field at point

1 is higher than that at point 2, where as point 1 is closer to the first coil 1 and the current value in the first coil is higher.

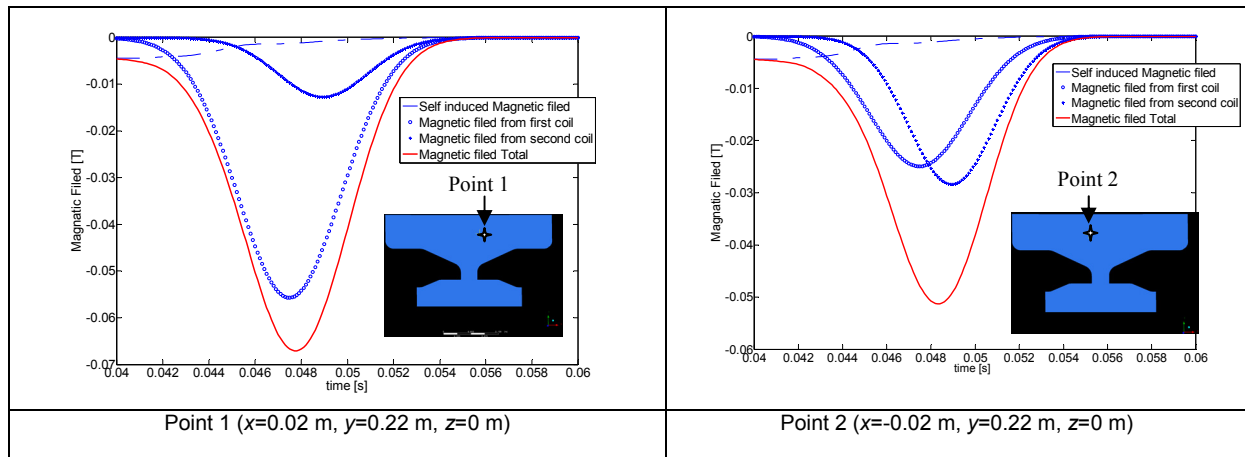


Fig.7 Magnetic field distribution versus time shown at two points.

5.2 Current and electric potential

An averaging of measured total current values in the circuit breaker is shown in Fig.8.a. The current decreases slowly in the first 43 ms since the electrical conductivity of air is very small during this period. The electrical conductivity of the air depends on the temperature and renders to zero at less than 5000 K (Capitelli et al 2002). In the period between 43 and 46 ms the current decreases sharply as the electrical conductivity of the air increases rapidly by the heating effect of the arc plasma. On the other hand, the elongation of the arc plasma increases the resistance to the electrical current, which explains the slow decrease of current in the period between 46 ms and 54 ms.

Fig 8.b-8d show different degrees of light emission measured by the optical sensors. The strength of the light reflects the strength of the current in the circuit. The light intensity spontaneously fluctuates with the time. Such instabilities in current increase the quenching of the charge in the high voltage wall as described by Smeets 1986.

Fig.8.b shows the decrease in the maximum value of the light emission, as the plasma arc moves from sensors 1 to sensor 4. The position of the sensors are illustrated in Fig.4. The arc time of flight from one point to another beside the high voltage plate can be estimated and the arc velocity can be approximated as

$$V_{\text{estimated}} = \frac{\text{Distance between the points}}{\text{The time of flight}} \quad (12)$$

The Reynolds number Re can be obtained from the relation:

$$Re = \frac{\rho V w}{\mu} \quad (13)$$

where w is the width of the channel. Some numerical examples are included in Table 2.

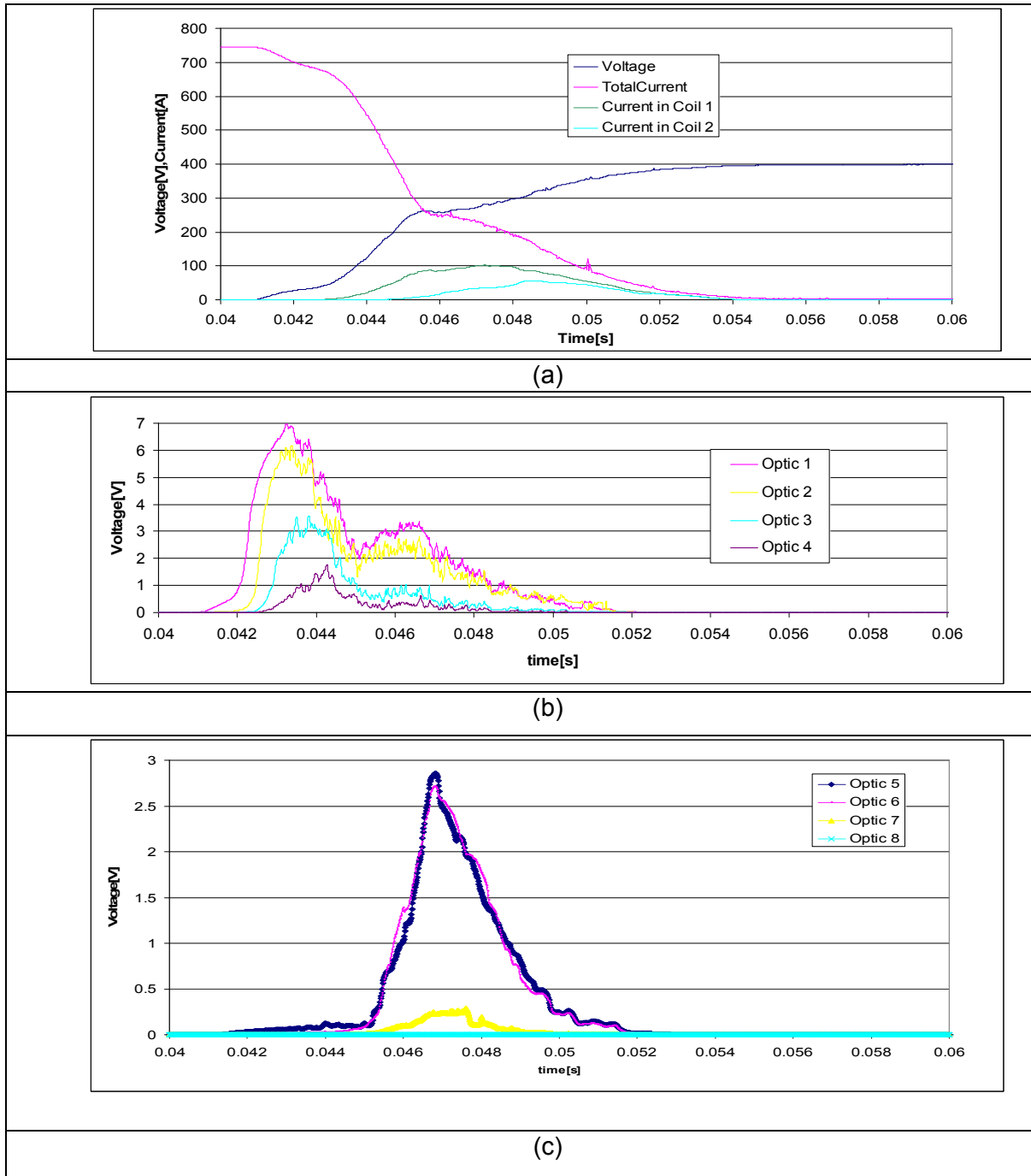
Table 2 Velocity and Reynolds number calculation

Sensor number	Distance between sensors (mm)	Time of flight (ms)	Velocity (m/s)	Re
2,3	13.088	0.439	29.81321	9536
3,4	12.392	0.452	27.41593	8773

The strength of the arc plasma generated at contact 2 is about 30% of its strength at contact 1. If you compare between Fig.8.b and Fig.8.c you see that the light appears first at contact 1 (represented by the optical sensors 1-4 in the former figure) then at contact 2

(represented by the optical sensors 5-8) in the later figure. The delay of the ignition time in contact 2 is due to the time of accumulation of the charges in the bridge plate. The arc plasma quenched completely after a very short time at sensor 8.

Fig. 8.d shows the strength of light at the horizontal located sensors 4, 9 and 10. The strength of voltage decreases from the anode at 4 to the middle position at 9 and becomes very low at position 10 near the low voltage contact.



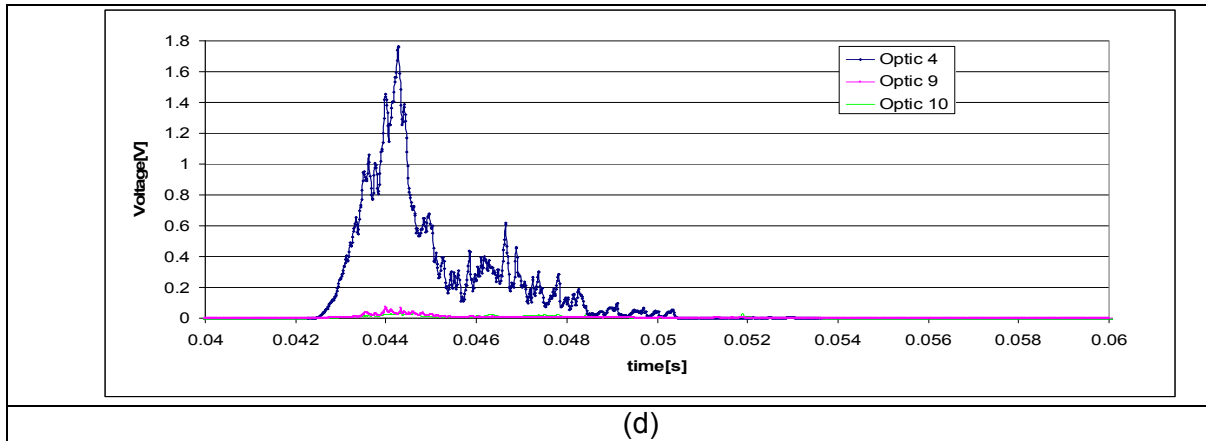


Fig. 8 (a) Average values of total current, voltage and current in measured in the coils. Figures (b-d) Light intensity measured by optical sensors located at different plates.

Fig. 9 shows the results for the voltage between plates A2 and B2 and the total current in a case of 180 A as an initial current. The current is computed by integrating the current density in plate A2. A close match can be seen between simulation and experimental data when the arc plasma starts to move between plates A2 and B2, i.e. at 0.171 s. Some differences appear between the experimental and numerical data in the initial period since the simulations do not cover the case that the arc moves along the bridge.

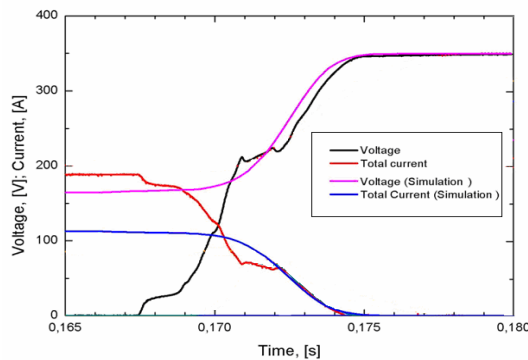


Fig.9 Voltage and the total current for a case with initial current of 180 A

5.3 Current Density, Magnetic Induction and Temperature

The current density, magnetic induction and temperature distribution in the symmetry plane is shown in Fig.10. The current density can be obtained from equation (6). It is clear from this figure that the current density increases with the temperature, due to the increase in the electrical conductivity. This result agrees with the Ohmic heating equation. Also, as expected from equation (8), Fig.10.c shows that the self-induced magnetic field increases by increasing the current density.

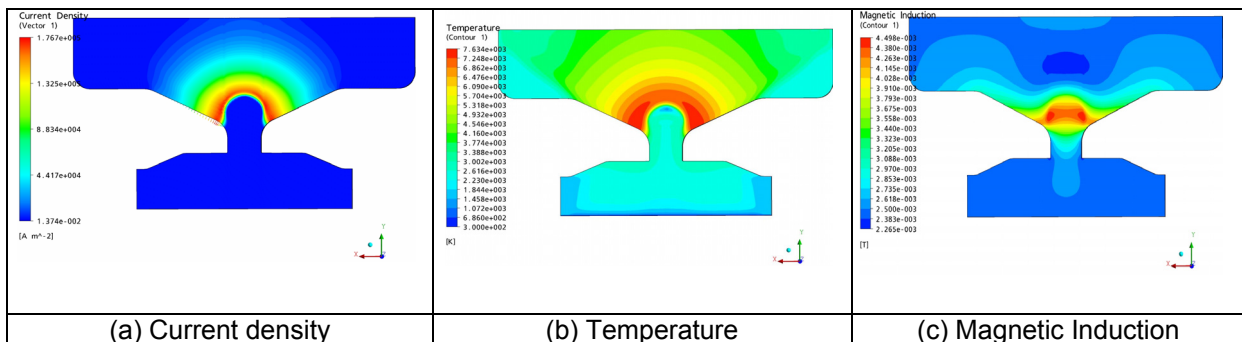


Fig.10 Distributions of the current density, temperature and magnetic field obtained at 48.8 ms for an initial current of 755 A.

The arc plasma development is shown in Fig.11. The maximum value of the arc current density reaches about $4.103 \times 10^5 \text{ A/m}^2$ at 36.4 ms. This value then reduces to $5.518 \times 10^2 \text{ A/m}^2$ at 47.5 ms due to the elongation of the arc plasma.

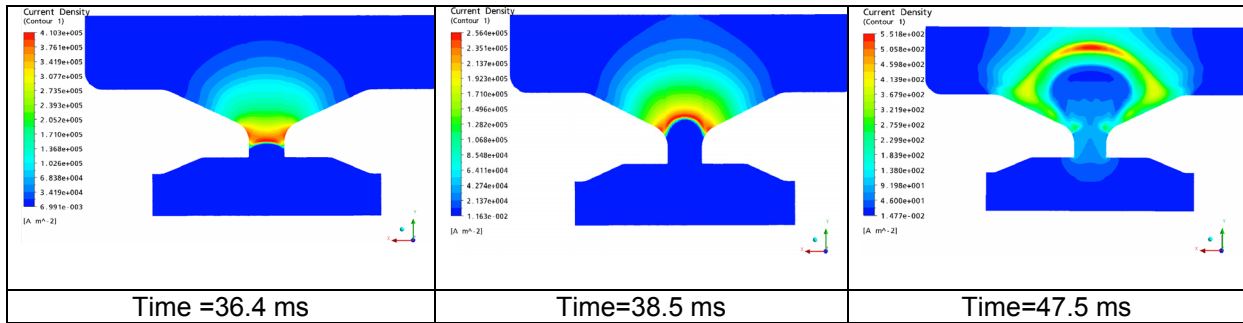


Fig. 11 Current density (A/m^2) of the arc plasma at different time instants for an initial current of 755 A.

5.4 Velocity of the arc plasma

The position of the arc plasma is obtained by computing the centre of the plasma current intensity along a line of symmetry. That is attained in the simulation by the equation:

$$\text{Arc position} = \frac{\oint y J_x dy}{\oint J_x dy} \quad \text{line 1-2} \quad (12)$$

Here, line 1-2 is the line of symmetry shown in Fig.12. This figure shows the arc plasma position and its velocity as a function of time. The velocity starts to increase until reaching point $y=0.19 \text{ m}$. The shape of the electrical breaker affects the velocity, e.g. by quenching the arc plasma. The velocity starts to decrease after $y=0.19 \text{ m}$, because the viscous forces and the turbulent mixing entrains more air around the plasma, which causes an increase in the mass of the flow.

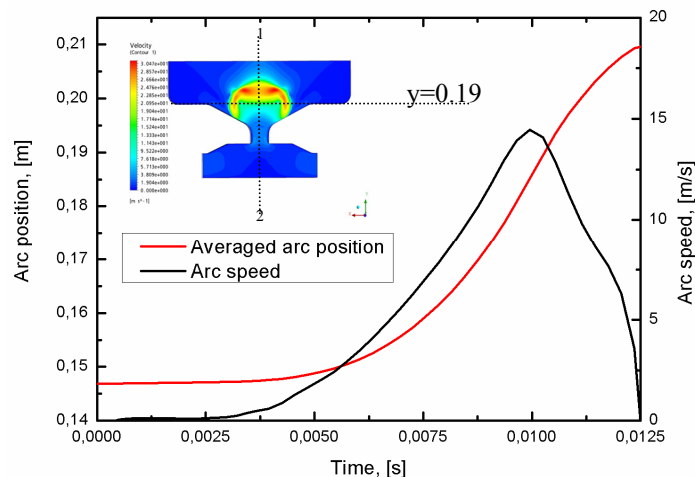


Fig.12 The arc plasma position and velocity at current of 180 A.

6. Conclusions

This paper provides a numerical and experimental study of an industrial electrical breaker. A 3-D model was investigated in which an additional magnetic field is generated from coils located near the runners of the breaker which help leading the ionized air between the runners.

In the configuration of the electrical breaker in the present work, the current flow depends on the temperature and the area of the arc plasma. The impacts of temperature and electrical conductivity on the induced magnetic field have been studied.

The effect of the self-induced magnetic field was shown to have much lower influence than that of the coils induced field. The magnetic field from the coil located near the high voltage plate was higher than that of the second coil.

From the optical analysis the Reynolds number of the plasma near the anode between the sensors 3 and 4 was about 9536, i.e. turbulence flow. Moreover, the velocity between parallel plates A2 and B2 was about 29.8 m/s, which reduces to about 27m/s when the plates diverge and the arc plasma elongates. The velocity starts to decrease after $y=0.19$ m because the viscous forces and the turbulent mixing inside the arc plasma drag more air around it which causes an increase in the mass of the flow.

The next step will be to develop a numerical model of the base of the electrical breaker including the effect of the magnetized material and the effect of the plates connected to the magnetized material.

7. Acknowledgments

We gratefully acknowledge the Bayerische Forschungsförderung for their financial support. This work has been done in cooperation with the Erlangen Graduate School in Advanced Optical Technologies (SAOT).

8. References

- ABB SACE (2003): "Electrical installation handbook", 1st edition, Bergamo (Italy), Page 115.
- Karetta .F., M. Lindmayer (1998): "Simulation of the gasdynamic and electromagnetic processes in low voltage switching arcs", IEEE Trans. CPMT-21 Part A Page. 96-103.
- Lindmayer. M, Marzahn. E, Mutzke.A, Rütter.T, and Springstubbe.M (2006): "The process of arc splitting between metal plates in low voltage arc chutes", IEEE Transactions on Components and Packaging Technologies, VOL. 29, NO. 2. Page 310.
- Lindmayer.M, Springstubbe.M: "3D-Simulation of arc motion including the influence of ferromagnetic material". 47th IEEE Holm, Conference on Electrical Contacts, Montreal 2001.
- Swierczynski B, J J Gonzalez, P Teulet , P Freton and A Gleizes (2004):" Advances in low voltage circuit breakers modelling" . Journal of physics D: Applied physics,37, pages 595-609.
- Capitelli. M, Colonna, G, Angola A.D (2001): "Thermodynamic properties and transport coefficients of high-temperature air plasma", IEEE,Vol 1, Pages 694- 697.
- Schlitz. L. Z., Garimella.S , Chan.S. (1999): "Gas dynamics and electromagnetic process in high-current arc plasma- part 1: model formulation and steady-state solution", Journal of applied physics , volume 85,Number 5. Page 2540.

Wu.Y, Rong.M , Lou.J. (2006): "Calculation of electric and magnetic fields in simplified chambers of low-Voltage circuit breakers", IEEE Transaction on magnetic, vol. 42,No 4, page 1007

Marandi.S (1996): "The magnetic near-field of a solenoid", IEEE Electrical and Computer Engineering, Canadian Conference, pp.1-4.

Smeets.R (1986): "Stability of low-current vacuum arcs", J. Phys. D: Appl. Phys. 19, Page 575-587.

Kralik, R. (2007): "Schütz für Gleichstrom- und Wechselstrombetrieb", EUROPÄISCHE PATENTANMELDUNG DE 102006035844.